

Comparison of LSTM autoencoder based deep learning enabled Bayesian inference using two time series reconstruction approaches

Saumik Dana^a

^a*University of Southern California,*

Abstract

In this work, we use a combination of Bayesian inference, Markov chain Monte Carlo and deep learning in the form of LSTM autoencoders to build and test a framework to provide robust estimates of injection rate from ground surface data in coupled flow and geomechanics problems. We use LSTM autoencoders to reconstruct the displacement time series for grid points on the top surface of a faulting due to water injection problem. We then deploy this LSTM autoencoder based model instead of the high fidelity model in the Bayesian inference framework to estimate injection rate from displacement input.

Keywords: LSTM autoencoder, Bayesian inference, Markov chain Monte Carlo, coupled flow and geomechanics

1. Introduction

The high fidelity forward model for coupled flow and geomechanics [1–8] in the absence of inertia is a piece of the puzzle in which forward simulations are used to arrive at the seismic impact of fault slip on earthquake activity. Typically, the earthquakes are measured with seismograms/geophones on the surface as P-waves and S-waves, and then these readings are used to calibrate the seismic activity for constant monitoring. The acceleration/displacement field around the fault slip activity translates to these waves recorded on the surface, and forward simulations with wave propagation bridge that gap. That being said, a seismic recording on the surface cannot easily be backtraced to the source of the fault slip. That is precisely inverse modeling, and the Bayesian framework coupled with Markov chain Monte Carlo [9] allows us to put such a framework in place. The accelerations/displacements are field quantities, and the inverse estimation of the field around the fault from the time series at the seismogram/geophone is not a trivial task. With that in mind, we test the robustness of the Bayesian/MCMC framework to inversely estimate a value instead of a field. To run Bayesian though, we need multiple (sometimes millions of) high fidelity simulation runs, which will become infeasible if the model is sophisticated. Hence, reduced order models are needed, and we deploy LSTM autoencoders for that purpose. In this work, we go from the forward model to the simulations to the time series data for the ground surface data, then LSTM autoencoder based reconstruction for an archetypal faulting due to injection problem, and then eventually Bayesian inference estimation of injection rate using the constructed reduced order model. The big picture scenario is that the recording at the seismogram/geophone would be fed into the Bayesian/MCMC framework as an input, and

the framework would provide an estimate of whichever model parameters are critical. The procedural framework is elucidated in the following steps

- Run high fidelity simulations for a bunch of injection rates
- For each injection rate, construct a displacement time series at a chosen grid point on the ground surface
- Add noise to the time series to eventually serve as noisy data for the Bayesian inference framework
- Train the LSTM autoencoder with time stamp and injection rate as input and displacement time series (without the noise) as the target
- Run the Bayesian inference framework on the noisy data with the LSTM autoencoder based reduced order model
- Test the robustness of the framework by comparing the estimates of the injection rate with the ground truth injection rate

1.1. Water injection in the presence of fault

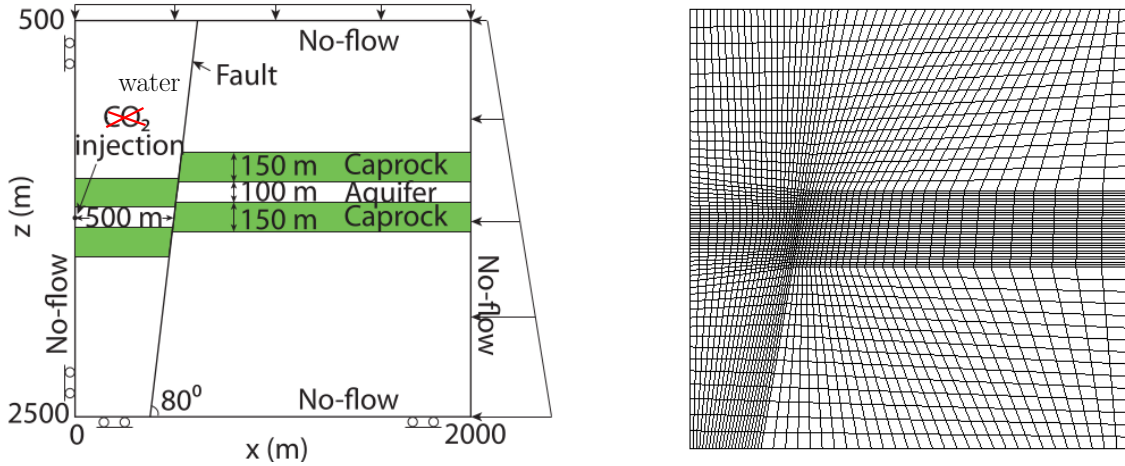


Figure 1: Model of the water injection plane strain case [10]) and the mesh of 3127 nodes and 3016 elements with more refinement around the fault

As shown in Fig. 1, we consider a two-dimensional plane-strain model with the fault under normal faulting conditions, that is, the vertical principal stress due to gravity is the largest among the three principal stresses. The mathematics and numerics of the forward model is explained in Appendix A. The aquifer is hydraulically compartmentalized with a sealing fault that cuts across it. The storage capacity of the aquifer is limited by overpressurization and slip on the fault. The initial fluid pressure at 500 m depth is 5 MPa and 24.63 MPa at 2500 m, considering a hydrostatic gradient of 9.81 MPa/km and an atmospheric pressure of 0.1 MPa at the ground surface. The rock density is 2260 kg/m³, so the lithostatic gradient is 22.17 MPa/km. Assuming a porosity of 0.1, the initial vertical stress is $11.085 \times 0.9 + 5 \times 0.1 = 10.4765$ MPa at 500 m, and $22.17 \times 2.5 \times 0.9 + 24.63 \times 0.1 = 52.3455$ MPa at 2500 m. We choose a value of 0.7 for the ratio of horizontal to vertical initial total stress. The average bulk density is $\rho_b = 2260 \times 0.9 + 1000 \times 0.1 = 2134$ kg/m³, the average sonic compressional and shear velocities are $V_p = 730$ m/s and $V_s = 420$ m/s respectively. The Biot coefficient is assumed to be $b = 1.0$. The friction coefficient drops linearly from static friction $\mu_s = 0.5$

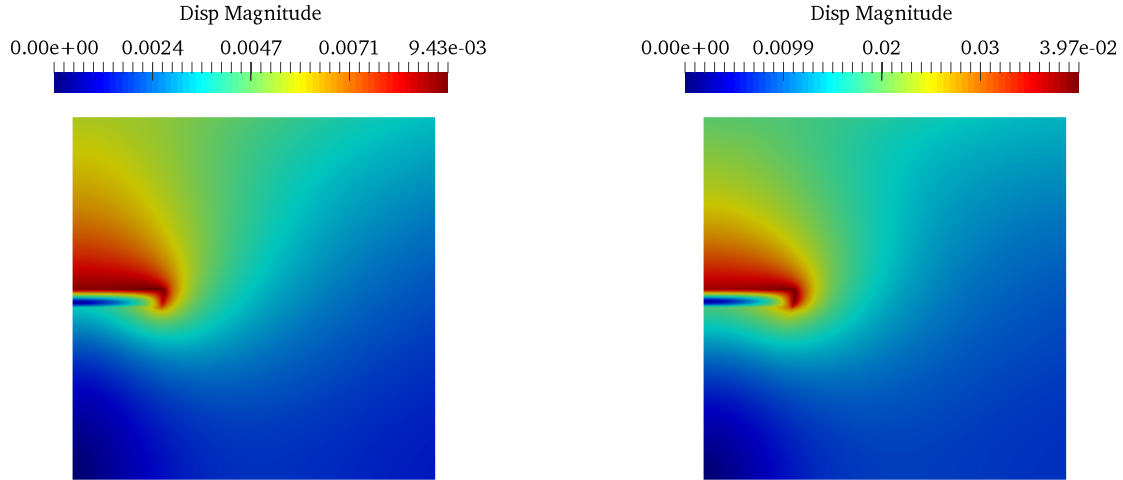


Figure 2: Snapshots of displacement at $t=60$ days for injection rates of 100 MSCF/day and 400 MSCF/day respectively

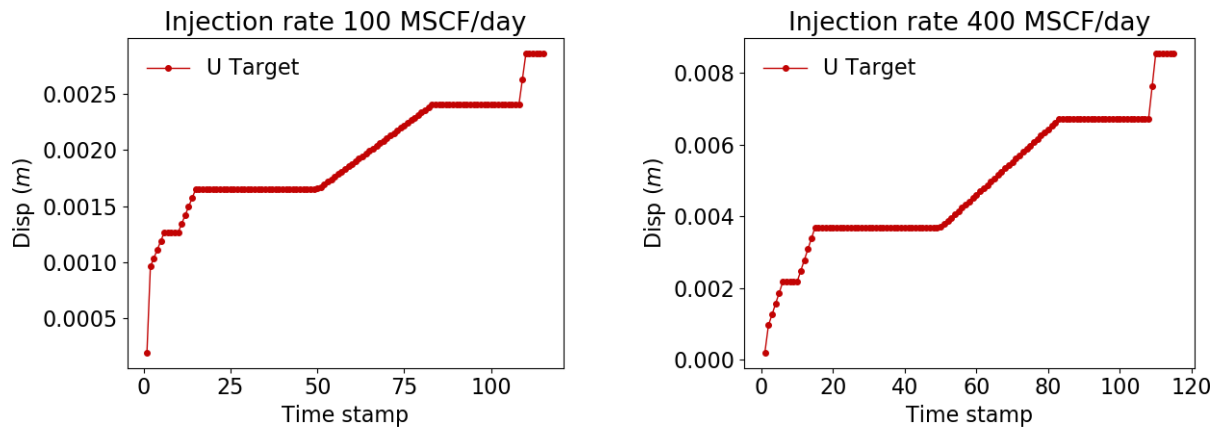


Figure 3: Displacement time series ground truth for u at $(0, 500)$ for injection rates on either end of the data spectrum.

to dynamic friction $\mu_d = 0.2$ over $d_c = 5 \text{ mm}$. Snapshots of the displacement evolution are given in Fig. 2. The simulator spits out vtk files for each time stamp in the simulation. Our job is to extract the displacement values corresponding to grid points on the top surface, and construct a time series as the ground truth, as shown in Fig. 3. A code snippet for processing vtk files is provided in Listing 1.

```

1 class parse_vtk:
2 # Base class for parsing vtk files
3
4 def get_surface_information(self, vector_name):
5     """
6     :vector_name: the vector you want to process
7     :return: displacement components
8     """

```

```

9     reader = vtk.vtkDataSetReader()
10    reader.SetFileName(self.infile)
11    reader.Update()
12    data = reader.GetOutput()
13    npoints = data.GetNumberOfPoints()
14    d = data.GetPointData()
15    array = d.GetArray(vector_name)
16
17    u, v, w, x, y, z = np.zeros(npoints), np.zeros(npoints), np.zeros
(npoints), np.zeros(npoints), np.zeros(npoints), np.zeros(npoints)
18
19    for n in range(npoints):
20        x[n], y[n], z[n] = data.GetPoint(n)
21        u[n], v[n], w[n] = array.GetTuple(n)
22
23    # Surface information at min x and max y
24    u = u[np.where((x==min(x)) & (y==max(y)))[0]]
25    v = v[np.where((x==min(x)) & (y==max(y)))[0]]
26
27    del x, y, z
28    return np.sqrt(u**2+v**2)

```

Listing 1: Code for processing vtk files

2. Reconstruction using LSTM autoencoders

A reduced order model would effectively mean reconstructing this time series using LSTM autoencoder, and the optimal deep learning parameters to best reconstruct the time series. The deep learning piece is built on the PyTorch framework, and all simulations are run on a basic AMD Ryzen 3 3200U with Radeon Vega Mobile Gfx \times 4 processor. A code snippet is provided in Listing 2.

```

1  class lstm_encoder(nn.Module):
2  # Encodes time-series sequence
3
4      def __init__(self, input_size, hidden_size, num_layers):
5          super(lstm_encoder, self).__init__()
6          self.lstm = nn.LSTM(input_size = input_size, hidden_size=
hidden_size, num_layers = num_layers)
7
8      def forward(self, x_input):
9          # called internally by PyTorch
10         lstm_out, self.hidden = self.lstm(x_input.view(x_input.shape
[0], x_input.shape[1], self.input_size))
11         return lstm_out, self.hidden
12
13  class lstm_decoder(nn.Module):
14  # Decodes hidden state output by encoder

```

```

15 def __init__(self, input_size, hidden_size, num_layers):
16     super(lstm_decoder, self).__init__()
17     self.lstm = nn.LSTM(input_size = input_size, hidden_size =
18 hidden_size, num_layers = num_layers)
19     self.linear = nn.Linear(hidden_size, input_size)
20
21 def forward(self, x_input, encoder_hidden_states):
22     # called internally by PyTorch
23     lstm_out, self.hidden = self.lstm(x_input.unsqueeze(0),
24 encoder_hidden_states)
25     output = self.linear(lstm_out.squeeze(0))
26     return output, self.hidden

```

Listing 2: LSTM autoencoder code snippet

2.1. Nonoverlapping window approach

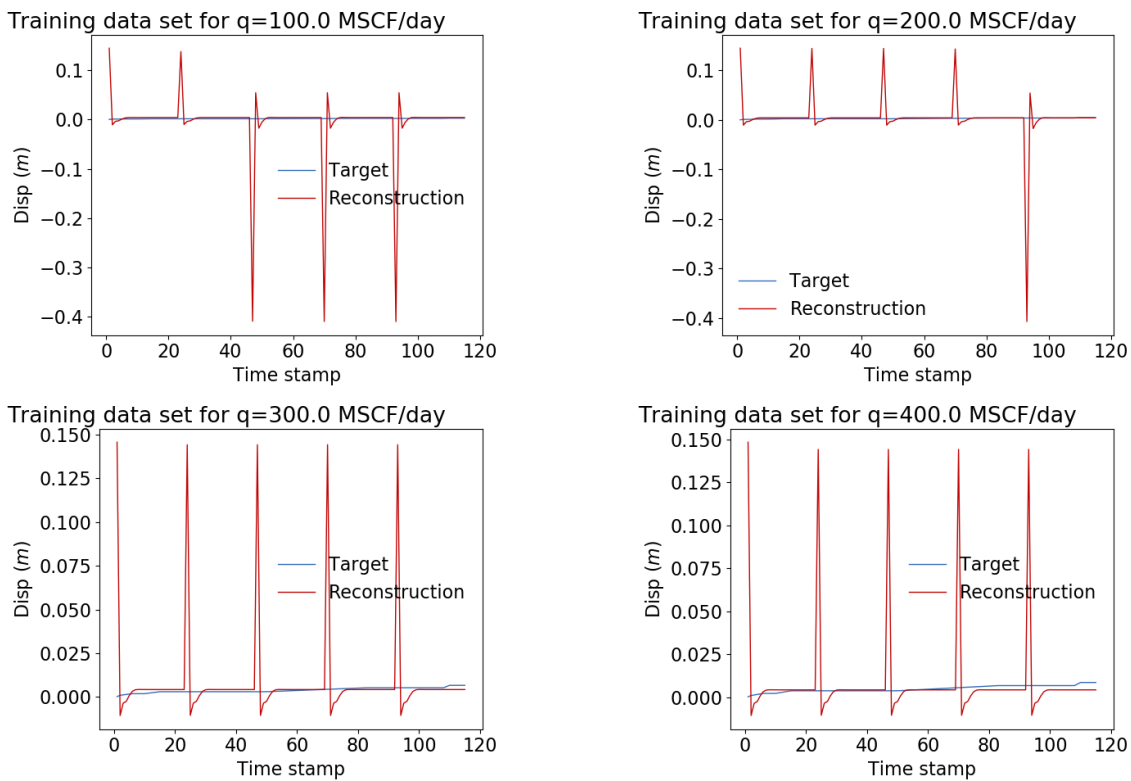


Figure 4: Reconstruction of displacement time series ground truth for u at $(0, 500)$ for different injection rates with nonoverlapping window approach

We use a window size of 23 for 115 time steps, hidden state size of 5, number of LSTM layers per encoder and decoder is 1, and we deploy the Adam optimizer to train the model using only 10 epochs to avoid overfitting. The 115 data points are divided exactly into windows of 23 data points, and the LSTM autoencoder is trained for these windows. During

reconstruction, these data chunks in the form of windows are fed into the trained LSTM autoencoder. The ratio of the window to the hidden state size is a measure of the amount of compression that is imposed while encoding the information using the encoder. We observe from Fig. 4 that the nonoverlapping window approach causes spikes in the reconstruction at the ends of each window. This is because the reconstruction at the start of a window does not carry information about the time series history from the end of the previous window. In order to smooth these spikes, we present the sliding window approach as explained below

2.2. Sliding window approach

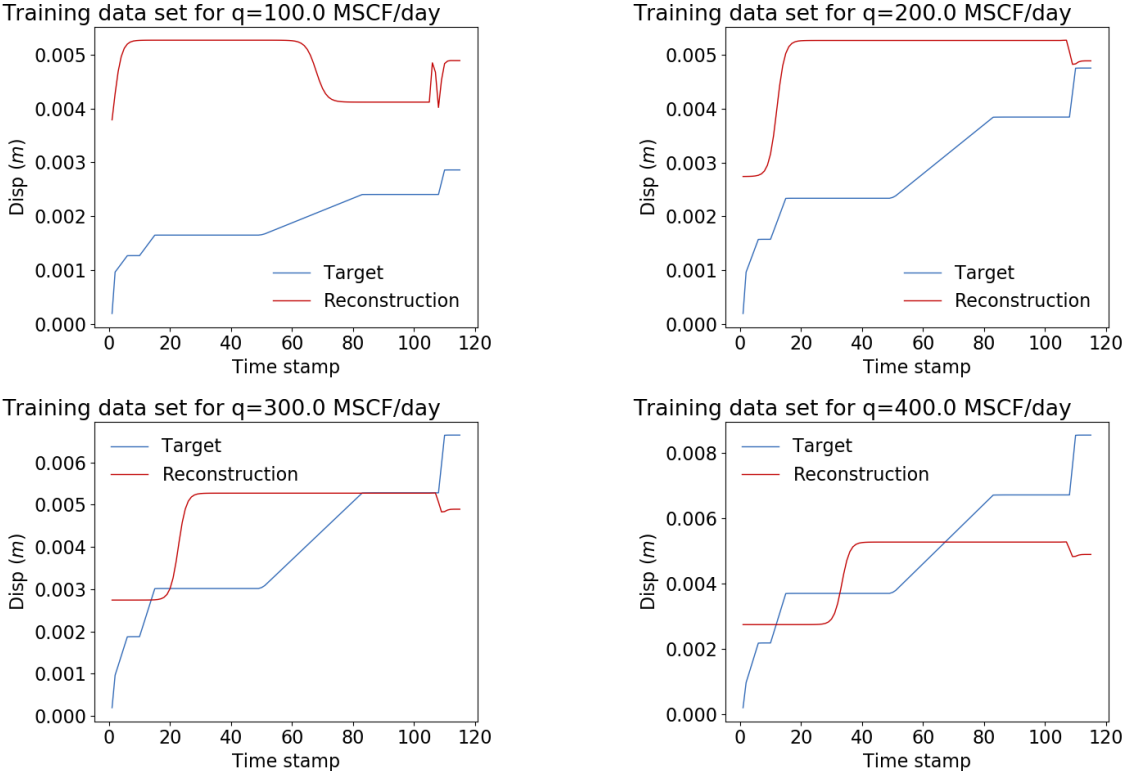


Figure 5: Reconstruction of displacement time series ground truth for u at $(0, 500)$ for different injection rates with sliding window approach

We use a window size of 10 for 115 time steps, hidden state size of 5, number of LSTM layers per encoder and decoder is 1, and we deploy the Adam optimizer to train the model using only 10 epochs to avoid overfitting. The 115 data points are divided into windows of 10 data points, and each window slides forward by 1, and the LSTM autoencoder is trained for these windows. During reconstruction, these data chunks in the form of windows are fed into the trained LSTM autoencoder. As we observe in Fig. 5, the sliding window approach allows the reconstructions over these overlaps to be averaged out, which smooths out the spikes that are observed in the nonoverlapping window approach. The reality is that the time series across the injection rates in the spectrum of the generated data spans an order of magnitude, and to fit all that into a LSTM autoencoder in a one size fits all manner is not a trivial task.

3. The formalism of Bayesian inference with Markov chain Monte Carlo sampling

The Bayesian inference framework works on the basic tent of uncovering a distribution centered around the true value and starts off with an initial guess for the distribution also called “prior” \mathcal{D} to eventually get to the most accurate distribution possible also called “posterior” \mathcal{P} through a likelihood \mathcal{L} . The Bayes theorem in a nutshell is:

$$\mathcal{P} = \frac{\mathcal{D} \times \mathcal{L}}{\int \mathcal{D} \times \mathcal{L}} \quad (1)$$

The prior is typically taken to be a Gaussian distribution and the likelihood carries information about the forward model. The quantity that makes evaluation of the posterior difficult is the integral term in the denominator. Since direct evaluation of the integral using quadrature rules is expensive, sampling methods like Markov chain Monte Carlo (MCMC) [11–14] are used. To put it mathematically, if we were evaluating an integral, then the sampling would apply to points at which we know the value of integrand, and then proceed to evaluate the integral. But if the integrand at each of those points is a distribution rather than a value, it makes the sampling and subsequent averaging significantly more complicated. By constructing a Markov chain that has the desired distribution as its equilibrium distribution, one can obtain a sample of the desired distribution by recording states from the chain. The more steps are included, the more closely the distribution of the sample matches the actual desired distribution.

3.1. Applied to our problem

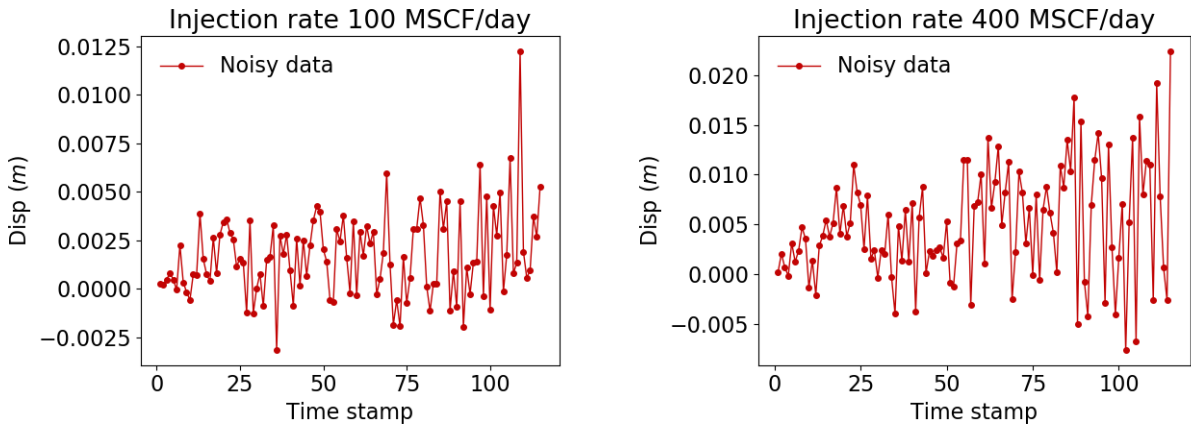


Figure 6: Displacement time series noisy data for u at $(2000, 500)$ for injection rates on either end of the data spectrum. The noisy data is generated from the ground truth using a Gaussian distribution

In this particular inverse problem, the displacement response of the model is known and the goal is to estimate the injection rate q . To formalize the problem, consider the relationship between displacement $u(t)$ and the forward model $\mathcal{F}(\theta)$ with model parameters, constants and variables θ by the following statistical model

$$u(t) = \mathcal{F}(\theta) + \epsilon \quad (2)$$

where ϵ is the noise. Assuming the $\epsilon \sim N(0, \sigma^2)$ as unbiased, independent and identical normal distribution with standard deviation σ allows us to conveniently generate the synthetic data as shown in Fig. 6. The goal of the inverse problem is to determine the model parameter distribution as follows

$$\pi(q|u(t_1), \dots, u(t_n)) = \frac{\pi(u(t_1), \dots, u(t_n)|q)\pi_0(q)}{\int_q \pi(u(t_1), \dots, u(t_n)|q)\pi_0(q)dq} \quad (3)$$

where $\pi_0(q)$ is the prior distribution and $\pi(u(t_1), \dots, u(t_n)|q)$ is the likelihood given by

$$\pi(u(t_1), \dots, u(t_n)|q) = \prod_{i=1}^n \pi(u(t_i)|q) = \prod_{i=1}^n \frac{1}{\sigma\sqrt{2\pi}} e^{-\frac{1}{2}\left(\frac{u(t_i)-\mathcal{F}(\theta)}{\sigma}\right)^2} \quad (4)$$

3.2. Adaptive metropolis algorithm

Algorithm 1: Metropolis-Hastings algorithm

```

1 m ← 0;
2 qm ← q0; // q0 is an initial guess
3 V ∼ qm; // Construct covariance matrix
4 for j=1,2,...,n do
5   q* ∼ qm, V; // Randomly sample from a distribution with covariance V
6   if q* ∉ (ql, qu) then
7     continue; // Move on if the guess is off the specified limits
8   else
9     γ ∼ q*; // Get standard deviation
10    if f(γ, q*) then
11      qm+1 ← q*; // Accept sample based on a condition f(γ, q*) being satisfied
12    else
13      qm+1 ← qm; // Reject sample
14  m ← m + 1;
15  if m % m0 then
16    V ∼ {qm, qm-1, ..., qm-m0}; // Update covariance matrix every m0 iterations

```

The adaptive Metropolis algorithm [13] explores the parameter space with specified limits ranging from a high of q^u to a low of q^l and starts from a random initial guess of the model parameter q^m , where m is the iteration number. The initial covariance matrix in the adaptive Metropolis algorithm is constructed using the initial parameter $q^{m=0}$. At each iteration, the steps are

1. A random parameter sample q^* is generated from the proposal distribution
2. If q^* is not within the specified limits, $q^* \notin (q^l, q^u)$, the iteration is passed without moving to the next steps, and the previous sample is considered as the new sample, $q^{m+1} = q^m$

3. If q^* is within the specified limits, $q^* \in (q^l, q^u)$, a new value of standard deviation associated with q^* is generated using the inverse-gamma distribution
4. q^* is accepted as the new sample $q^{m+1} = q^*$ if a criterion which involves the standard deviation is met
5. The covariance matrix is updated if the iteration number is an exact multiple of m_0 using the previous m_0 model parameters

The simulation is repeated for n iterations and the parameter samples resulting from all these iterations represent the parameter posterior distribution. The construction of the q^* is only based on the current parameter, q^m , which is the Markov process. The computational time of the MCMC sampling method is proportional to the number of generated samples n . To put it more succinctly, the algorithm is elucidated in Algorithm 1.

4. Results

The interval of adapting the covariance matrix is 100, which means the matrix is modified every 100 samples. Also, since the initial guess is more often than not way off the desired value, the initial half of the number of samples are burnt-in, which is common practice in MCMC simulations. We start with an initial guess of 1 MSCF/day for all Bayesian/MCMC simulations, which is way off the desired estimated value. In reality, this tests the robustness of the framework, as the initial guess in realistic scenarios is expected to be way off the desired estimated value because we do not know the desired estimated value.

4.1. Using the reduced order model obtained through nonoverlapping window approach

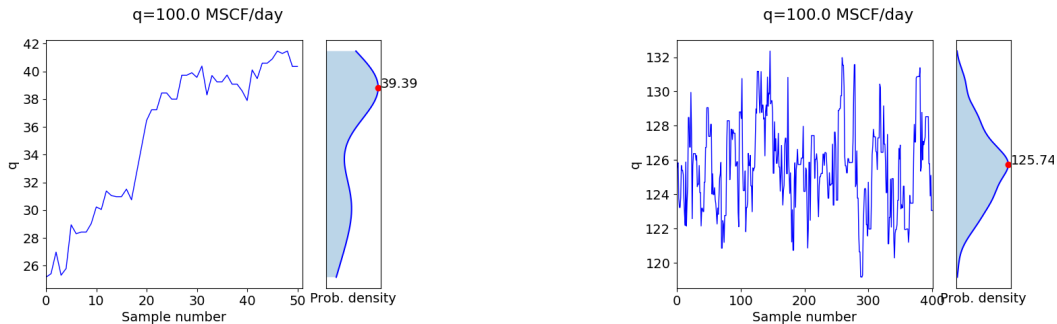


Figure 7: Inversion results for 100 MSCF/day with nonoverlapping window based reconstruction

Figs. 7- 10 are results of the Bayesian/MCMC inference framework for the different injection rates in the spectrum for different number of samples. We observe from the results that the estimation is evidently impacted by how good the reduced order model is in the first place, and we know from Fig. 4 that LSTM autoencoders do a lot better when the time series is oscillatory more than any other feature. We also observe that the estimation is not always monotonically converging to the ground truth with increasing number of samples, but is expected to beyond a certain number of samples, which is a function of the value itself, the reduced ordel model, and how well the reduced order model works for the value in and around the ground truth.

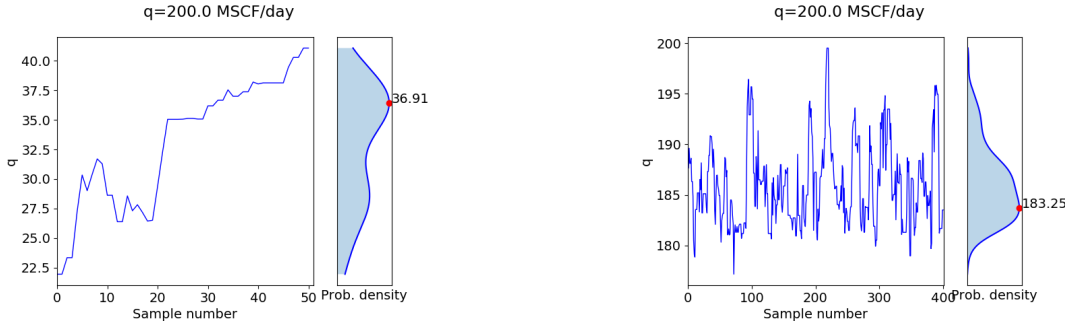


Figure 8: Inversion results for 200 MSCF/day with nonoverlapping window based reconstruction

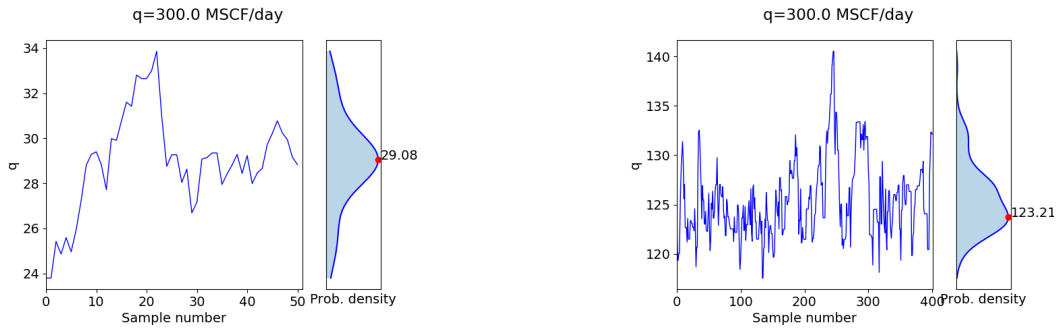


Figure 9: Inversion results for 300 MSCF/day with nonoverlapping window based reconstruction

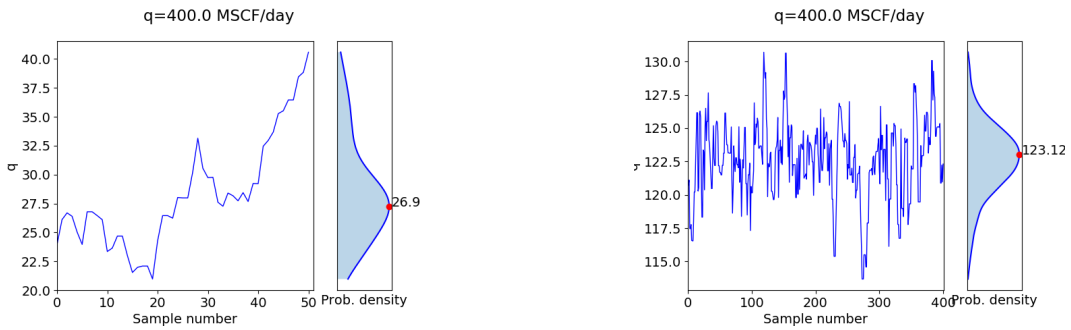


Figure 10: Inversion results for 400 MSCF/day with nonoverlapping window based reconstruction

4.2. Using the reduced order model obtained through sliding window approach

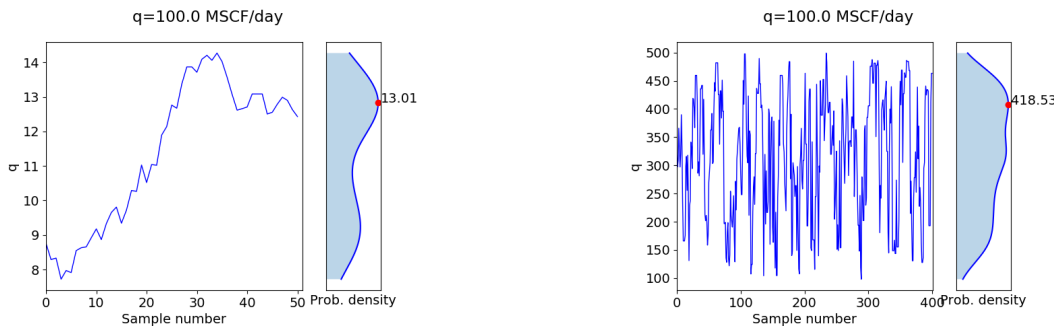


Figure 11: Inversion results for 100 MSCF/day with sliding window based reconstruction

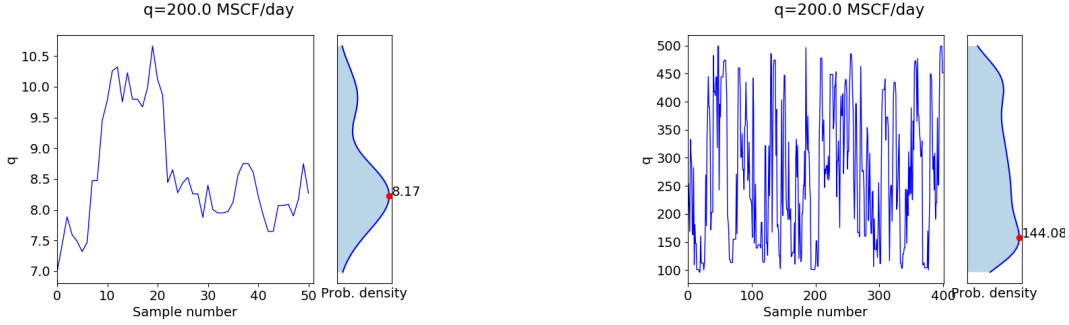


Figure 12: Inversion results for 200 MSCF/day with sliding window based reconstruction

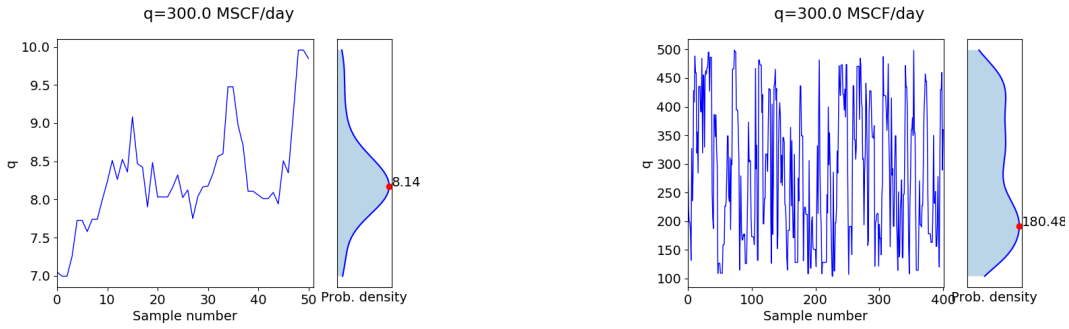


Figure 13: Inversion results for 300 MSCF/day with sliding window based reconstruction

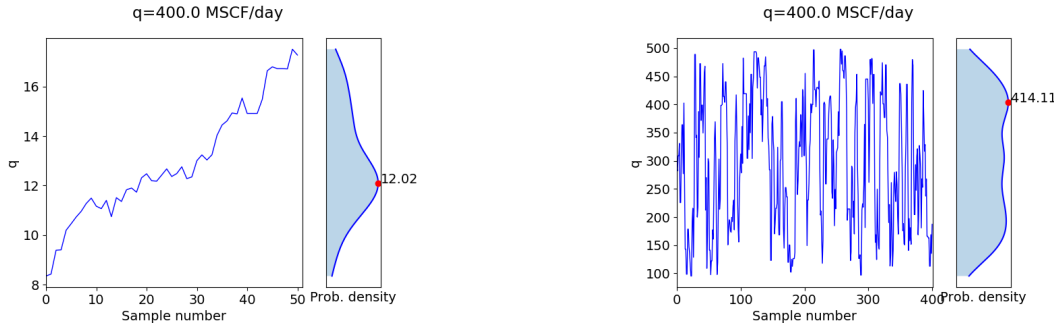


Figure 14: Inversion results for 400 MSCF/day with sliding window based reconstruction

Figs. 11- 14 are results of the Bayesian/MCMC inference framework for the different injection rates in the spectrum for different number of samples. Overall, the estimates with the sliding window based reconstruction is much better than the nonoverlapping window based reconstruction.

5. Conclusions and outlook

To summarise the procedural framework in this work again, the steps we followed were:

- Run high fidelity simulations for a bunch of injection rates
- For each injection rate, construct a displacement time series at a chosen grid point on the ground surface

- Add noise to the time series to eventually serve as noisy data for the Bayesian inference framework
- Train the LSTM autoencoder with time stamp and injection rate as input and displacement time series (without the noise) as the target
- Run the Bayesian inference framework with the LSTM autoencoder based reduced order model
- Test the robustness of the framework by comparing the estimates of the injection rate with the ground truth injection rate

We observed that the Bayesian/MCMC performance is squarely a function of how well the reduced order model replicates the high fidelity model, and while this is a good sign as the Bayesian/MCMC piece is robust, it lends to more future work in the realm of doing a good job of model order reduction. In this realm, decompositions play a role in the form of principal component analysis of the time stamps of the solution vector from the high fidelity, and it remains to be seen how to tie in that analysis into a sophisticated forward model using a framework like PyTorch. The author is aware of such frameworks being increasingly developed, and that is the ballpark in terms of future work of developing the software package.

Appendix A. The high fidelity forward model

The governing PDE for displacement \mathbf{u} is the linear momentum balance given by

$$\nabla \cdot \boldsymbol{\sigma} + \rho_b \mathbf{g} = \mathbf{0} \quad (\text{A.1})$$

with the constitutive laws relating poroelastic stress tensor $\boldsymbol{\sigma}$, effective stress tensor $\boldsymbol{\sigma}'$, strain tensor $\boldsymbol{\epsilon}$, volumetric strain $\epsilon = tr(\boldsymbol{\epsilon})$ and pore pressure p given by

$$\begin{aligned} \boldsymbol{\sigma} &= \boldsymbol{\sigma}' - bp\mathbf{I} \\ \boldsymbol{\sigma}' &= \lambda\epsilon\mathbf{I} + 2G\boldsymbol{\epsilon} = \mathbf{D}\boldsymbol{\epsilon} \end{aligned} \quad (\text{A.2})$$

with boundary and initial conditions given by

$$\begin{aligned} \mathbf{u} &= \bar{\mathbf{u}} \text{ on } \Gamma_D, \quad \dot{\mathbf{u}} = \dot{\bar{\mathbf{u}}} \text{ on } \Gamma_D, \quad \boldsymbol{\sigma}^T \mathbf{n} = \bar{\mathbf{t}} \text{ on } \Gamma_N \\ \mathbf{u}(\mathbf{x}, 0) &= \mathbf{u}_0(\mathbf{x}), \quad \dot{\mathbf{u}}(\mathbf{x}, 0) = \dot{\mathbf{u}}_0(\mathbf{x}) \end{aligned}$$

As shown in Fig. A.15, slip on the fault is the displacement of the positive side relative to the negative side:

$$(\mathbf{u}_+ - \mathbf{u}_-) - \mathbf{d} = \mathbf{0} \text{ on } \Gamma_f, \quad (\text{A.3})$$

Recognizing that fault tractions are analogous to the boundary tractions, we add in the contributions from integrating the Lagrange multipliers $\mathbf{l} \equiv \boldsymbol{\sigma}' \mathbf{n}$ over the fault surface in the conventional finite element formulation to get

$$\begin{aligned} & \int_{\Omega} \nabla \boldsymbol{\eta} : (\boldsymbol{\sigma}' - bp\mathbf{I}) \, d\Omega - \int_{\Omega} \boldsymbol{\eta} \cdot \rho_b \mathbf{g} \, d\Omega - \int_{\Gamma_N} \boldsymbol{\eta} \cdot \bar{\mathbf{t}} \, d\Gamma \\ & + \int_{\Gamma_{f+}} \boldsymbol{\eta} \cdot (\mathbf{l} - bp_+ \mathbf{n}) \, d\Gamma - \int_{\Gamma_{f-}} \boldsymbol{\eta} \cdot (\mathbf{l} - bp_- \mathbf{n}) \, d\Gamma = 0 \end{aligned} \quad (\text{A.4})$$

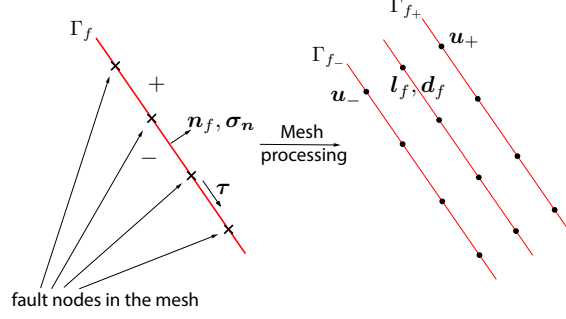


Figure A.15: A fault surface Γ_f is processed to create three surfaces: the positive side surface Γ_{f+} containing \mathbf{u}_+ , the negative side surface Γ_{f-} containing \mathbf{u}_- , and the slip surface containing the fault effective traction vector \mathbf{l} and the slip vector \mathbf{d}

We use the Mohr-Coulomb theory [15] to define the stability criterion for the fault and define a fault pressure $p_f = \frac{p_- + p_+}{2}$. The shear stress and frictional stresses on the fault are

$$\tau = |\mathbf{l} - \sigma'_n \mathbf{n}| \equiv |\mathbf{l} - (\mathbf{l} \cdot \mathbf{n}) \mathbf{n}|$$

$$\tau_f = \begin{cases} \tau_c - \mu_f \mathbf{l} \cdot \mathbf{n}, & \mathbf{l} \cdot \mathbf{n} < 0, \\ \tau_c, & \mathbf{l} \cdot \mathbf{n} \geq 0 \end{cases}$$

where τ_c is the cohesive strength of the fault, μ_f is the coefficient of friction which evolves as

$$\mu_f = \begin{cases} \mu_s - (\mu_s - \mu_d) \frac{|\mathbf{d}|}{d_c}, & |\mathbf{d}| \leq d_c, \\ \mu_d, & |\mathbf{d}| > d_c \end{cases} \quad (\text{A.5})$$

where d_c is a critical slip distance. The fields are approximated as follows:

$$\mathbf{u} \approx \mathbf{u}_h = \sum_{b=1}^{n_{\text{node}}} \eta_b \mathbf{U}_b, \quad \mathbf{l} \approx \mathbf{l}_h = \sum_{b=1}^{n_{f,\text{node}}} \eta_b \mathbf{L}_b, \quad \mathbf{d} \approx \mathbf{d}_h = \sum_{b=1}^{n_{f,\text{node}}} \eta_b \mathbf{D}_b,$$

where n_{node} is the total number of nodes and $n_{f,\text{node}}$ is the number of Lagrange nodes. After substitution of the finite element approximations into the weak form of the problem, we obtain the fully discrete aligns in residual form for all nodes a and lagrange nodes \bar{a} :

$$\mathbf{R}_{u,a}^{\text{Stat}} = \int_{\Omega} \mathbf{B}_a^T (\boldsymbol{\sigma}_h^{n+1} - b p_h^{n+1} \mathbf{1}) d\Omega - \int_{\Omega} \boldsymbol{\eta}_a^T \rho_{b,h}^{n+1} \mathbf{g} d\Omega - \int_{\Gamma_N} \boldsymbol{\eta}_a^T \bar{\mathbf{t}} d\Gamma$$

$$+ \int_{\Gamma_{f+}} \boldsymbol{\eta}_a^T (\mathbf{l}_h^{n+1} - b p_{f,h}^{n+1} \mathbf{n}) d\Gamma - \int_{\Gamma_{f-}} \boldsymbol{\eta}_a^T (\mathbf{l}_h^{n+1} - b p_{f,h}^{n+1} \mathbf{n}) d\Gamma = \mathbf{0} \quad (\text{A.6})$$

$$\mathbf{R}_{l,\bar{a}}^{\text{Stat}} = \int_{\Gamma_{f+}} \boldsymbol{\eta}_{\bar{a}}^T \mathbf{u}_{h+}^{n+1} d\Gamma - \int_{\Gamma_{f-}} \boldsymbol{\eta}_{\bar{a}}^T \mathbf{u}_{h-}^{n+1} d\Gamma - \int_{\Gamma_f} \boldsymbol{\eta}_{\bar{a}}^T \mathbf{d}_h^{n+1} d\Gamma = \mathbf{0} \quad (\text{A.7})$$

We find the system Jacobian matrix by isolating the term for the increments in displacements and Lagrange multipliers at time step $n+1$. The system of linear aligns is:

$$\begin{bmatrix} \mathbf{K}_{rr} & \mathbf{K}_{r+} & \mathbf{K}_{r-} & \mathbf{0} \\ \mathbf{K}_{+r} & \mathbf{K}_{++} & \mathbf{0} & \mathbf{C}_+^T \\ \mathbf{K}_{-r} & \mathbf{0} & \mathbf{K}_{--} & -\mathbf{C}_-^T \\ \mathbf{0} & \mathbf{C}_+ & -\mathbf{C}_- & \mathbf{0} \end{bmatrix} \begin{bmatrix} d\mathbf{U}_r \\ d\mathbf{U}_+ \\ d\mathbf{U}_- \\ d\mathbf{L} \end{bmatrix} = - \begin{bmatrix} \mathbf{R}_{u,r}^{\text{Stat}} \\ \mathbf{R}_{u,+}^{\text{Stat}} \\ \mathbf{R}_{u,-}^{\text{Stat}} \\ \mathbf{R}_l^{\text{Stat}} \end{bmatrix} \quad (\text{A.8})$$

Algorithm 2: Time-marching in poroelastostatics

```
1  $n \leftarrow 0; t \leftarrow 0;$ 
2  $\mathbf{d}_h^0 \leftarrow \mathbf{0};$  // Initialize fault slip at virgin state
3  $\mathbf{u}_h^0 \leftarrow \mathbf{u}_h^{Prestep};$  // Initial condition based on a elastic prestep solve
4 while  $t < T$  do
    /* time marching till final time */
5   while Not converged do
    /* Staggered solution algorithm loop */
6     Solve flow problem for pressures;
7      $\mathbf{d}_h^{n+1} \leftarrow \mathbf{d}_h^n;$  // Initialize fault slip for next time step
8     Solve system of aligns using GMRES; // Krylov subspace solver
9      $\mathbf{L} \leftarrow \mathbf{L} + d\mathbf{L};$  // Update lagrange multipliers
10     $\mathbf{U} \leftarrow \mathbf{U} + d\mathbf{U};$  // Update displacements
11    for Loop over lagrange nodes do
12       $\tau \leftarrow |\mathbf{l}_h^{n+1} - (\mathbf{l}_h^{n+1} \cdot \mathbf{n})\mathbf{n}|;$  // Obtain shear stress on fault
13       $\tau_f \leftarrow \tau_f |d_h^n|;$  // Compute fault friction based on the slip value at
        previous time step
14      while  $\tau > \tau_f$  do
        /* Satisfy fault constitutive law */
15         $\mathbf{U}_+ \leftarrow \mathbf{U}_+ - \mathbf{K}_{++}^{-1} \frac{\tau - \tau_f}{\tau} \mathbf{L};$ 
16         $\mathbf{U}_- \leftarrow \mathbf{U}_- + \mathbf{K}_{--}^{-1} \frac{\tau - \tau_f}{\tau} \mathbf{L};$ 
17         $\mathbf{d}_h^{n+1} \leftarrow \mathbf{u}_{h_+}^{n+1} - \mathbf{u}_{h_-}^{n+1};$  // Update fault slip
18         $\tau_f \leftarrow \tau_f |d_h^{n+1}|;$  // Update fault friction
19         $\mathbf{d}_h^{n+1} \leftarrow \mathbf{u}_{h_+}^{n+1} - \mathbf{u}_{h_-}^{n+1};$  // Update fault slip
20     $n \leftarrow n + 1;$ 
21     $t \leftarrow t + \Delta t;$ 
```

where the top row corresponds to displacement nodes excluding the fault positive and negative side nodes. In many quasi-static simulations it is convenient to compute a static problem with elastic deformation prior to computing a transient response. The heavy lifting for the time marching is done at the Krylov solver [16] stage to solve the system of Eqs. (A.8) as shown in Algorithm 2.

References

- [1] S. Dana, M. F. Wheeler, Convergence analysis of fixed stress split iterative scheme for anisotropic poroelasticity with tensor biot parameter, *Computational Geosciences* 22 (2018) 1219–1230.
- [2] S. Dana, M. F. Wheeler, Convergence analysis of two-grid fixed stress split iterative scheme for coupled flow and deformation in heterogeneous poroelastic media, *Computer Methods in Applied Mechanics and Engineering* 341 (2018) 788–806.

- [3] S. Dana, B. Ganis, M. F. Wheeler, A multiscale fixed stress split iterative scheme for coupled flow and poromechanics in deep subsurface reservoirs, *Journal of Computational Physics* 352 (2018) 1–22.
- [4] S. Dana, S. Srinivasan, S. Karra, N. Makedonska, J. D. Hyman, D. O’Malley, H. Viswanathan, G. Srinivasan, Towards real-time forecasting of natural gas production by harnessing graph theory for stochastic discrete fracture networks, *Journal of Petroleum Science and Engineering* 195 (2020) 107791.
- [5] S. Dana, M. Jammoul, M. F. Wheeler, Performance studies of the fixed stress split algorithm for immiscible two-phase flow coupled with linear poromechanics, *Computational Geosciences* (2021) 1–15.
- [6] S. Dana, J. Ita, M. F. Wheeler, The correspondence between voigt and reuss bounds and the decoupling constraint in a two-grid staggered algorithm for consolidation in heterogeneous porous media, *Multiscale Modeling & Simulation* 18 (2020) 221–239.
- [7] S. Dana, Addressing challenges in modeling of coupled flow and poromechanics in deep subsurface reservoirs, Ph.D. thesis, The University of Texas at Austin, 2018.
- [8] L. Gasparini, J. R. Rodrigues, D. A. Augusto, L. M. Carvalho, C. Conopoima, P. Goldfeld, J. Panetta, J. P. Ramirez, M. Souza, M. O. Figueiredo, V. M. Leite, Hybrid parallel iterative sparse linear solver framework for reservoir geomechanical and flow simulation, *Journal of Computational Science* 51 (2021) 101330.
- [9] A. Olivier, D. G. Giovanis, B. Aakash, M. Chauhan, L. Vandanapu, M. D. Shields, Uqpy: A general purpose python package and development environment for uncertainty quantification, *Journal of Computational Science* 47 (2020) 101204.
- [10] F. Cappa, J. Rutqvist, Impact of CO₂ geological sequestration on the nucleation of earthquakes, *Geophys. Res. Lett.* 38 (2011) L17313.
- [11] A. Shapiro, Monte carlo sampling methods, *Handbooks in operations research and management science* 10 (2003) 353–425.
- [12] W. K. Hastings, Monte Carlo sampling methods using Markov chains and their applications, Oxford University Press, 1970.
- [13] H. Haario, E. Saksman, J. Tamminen, An adaptive metropolis algorithm, *Bernoulli* (2001) 223–242.
- [14] C. L. Mueller, Exploring the common concepts of adaptive MCMC and Covariance Matrix Adaptation schemes, 2010.
- [15] J. C. Jaeger, N. G. W. Cook, *Fundamentals of Rock Mechanics*, Chapman and Hall, London, 1979.
- [16] H. A. Van Der Vorst, Krylov subspace iteration, *Computing in science & engineering* 2 (2000) 32–37.